Monte Carlo Simulations Investigating the Threading of Cyclic Poly(ethylene oxide) by Linear Chains in the Melt

Carin A. Helfer, Guoqiang Xu, Wayne L. Mattice,* and Coleen Pugh

Institute of Polymer Science, The University of Akron, Akron, Ohio 44325-3909

Received March 27, 2003; Revised Manuscript Received July 9, 2003

ABSTRACT: A coarse-grained Monte Carlo algorithm on a modified diamond lattice has been used to study the dependence of threading of cyclic poly(ethylene oxide) molecules by linear poly(ethylene oxide) chains in the melt on the mass fraction (X_c) and the size (N_c) of the cyclics. Both short-range interactions based on the rotational isomeric state model and long-range interactions from a discretized form of the Lennard-Jones (LJ) potential energy function are included. LJ parameters σ and ϵ/k_B of 3.76 Å and 154 K, respectively, are estimated for the coarse-grained model. In addition, a method is presented for detecting threading of cyclics that have instantaneous conformations that significantly differ from a circle. The percentage of cyclic molecules threaded can be described as a linear function of X_c. When the cyclics consist of 10 or less coarse-grained monomer units, the percentage of cyclic molecules threaded falls to less than 1%, which suggests that spontaneous threading of cyclics smaller than 30-crown-10 is impractical in the melt. In addition, multiple threading occurs in cyclics larger than 42-crown-14. A weak end effect causes a slight preference for threading near the chain end.

Introduction

A rotaxane consists of a cyclic component threaded by a linear molecule that is held in place with bulky stopper groups at both ends to prevent unthreading.[1−11] If no stopper groups are present to lock in the threading, a pseudorotaxane results. Because of the unique nature of these structures and the lack of a covalent bond between the cyclic and linear components, these structures are predicted to have interesting properties that differ from the properties of the initial starting materials.[6,12] Therefore, many potential uses exist for these materials including improved interfacial adhesion and processability, control of thermal properties, viscosity, and molecular ordering.[6] In addition, electro- and photochemically active structures are possible.

Computational studies have provided insight into the formation of rotaxanes. Rotational isomeric state (RIS) theory and Monte Carlo (MC) methods were used to study the dependence of threading on the size of the cyclic molecules of poly(dimethylsiloxane), PDMS.[13,14] Also, the size and conformations of crown ethers as a function of solvent polarity were investigated using MC simulations.[15] The process known as shuttling, which is the movement of the macrocyclic component along the dumbbell-shaped component of the rotaxane, was investigated using molecular dynamics simulations,[16,17] molecular mechanics calculations,[17] and a one-dimensional quantum mechanical model.[18] In addition, MC simulations were used to study the kinetics of the threading of the cyclics onto the polymer chain, which can be described as a consecutive hopping process[19] as well as to study the influence of the stopper geometry on rotaxane yield.[20]

Previously, homopolyrotaxanes of poly(ethylene oxide), PEO, were investigated using an amphiphilic approach.[21] In the current study, we perform coarse-grained MC simulations to study pseudorotaxanes consisting of the threading of cyclic PEO molecules by linear PEO chains in the melt. The dependence of threading of the cyclic PEO molecules by the linear PEO chains on the mass fraction (X_c) and the size (N_c) of the cyclics is evaluated.

The simulations are performed on the 2nnd (second nearest neighbor diamond) lattice, which is a high coordination lattice for which the coarse-grained chains can be reverse-mapped into fully atomistic models in continuous space.[22−24] The use of coarse-graining and lattice models enables the simulation of large polymer systems with long relaxation times. Equilibration of the degree of threading in this polymer system was impossible with the currently available computer resources when an atomistically detailed model was used (Clancy and Mattice, unpublished). In the present simulations, the system equilibrates relatively quickly, allowing for the equilibrium properties to be evaluated.

In the simulations, short-range interactions are based on the RIS model and long-range interactions are based on a LJ potential energy function. In our model, the level of coarse-graining treats two backbone atoms (either C−C or C−O) as one bead on the lattice with the C and O treated equally in the long-range interactions. Using this approximation, we initially estimate the LJ parameters, σ and ϵ, since these parameters for our specific level of coarse-graining are not available in the literature. Presented first are the methods of estimating the LJ parameters since these parameters are crucial to the construction of the model of PEO melts.

The simulation includes results for cyclics that are large enough so that their instantaneous conformations are poorly approximated by a circle. A circle has principal moments of the radius of gyration tensor given by $L_1^2 = L_2^2 > 0$, $L_3^2 = 0$, whereas the larger cyclics in the simulation have averaged principal moments given by $\langle L_1^2\rangle > \langle L_2^2\rangle > \langle L_3^2\rangle > 0$. We describe a method that detects threading with these cyclics that have instantaneous conformations different from a circle.

Simulation Method and Details

Model. The MC simulations are performed on a high coordination lattice[22] using coarse-grained PEO chains.[23]

10.1021/ma0301855 CCC: $25.00
Published on Web 11/26/2003

Table 1. First- and Second-Order Interactions of a RIS Model of Poly(ethylene oxide)[25]

interaction	kJ/mol
$E\sigma_{AA}$	3.2
$E\sigma_{BB}$	−2.2
$E\omega_{AA}$	∞
$E\omega_{AB}$	2.2

This lattice, which can be constructed by eliminating every other site from a diamond lattice, has a coordination number of 12, which provides flexibility to define a rotational state on the lattice. A cyclic or chain with $2a$ non-hydrogen atoms is represented by a cyclic or chain of a coarse-grained beads, connected by coarse-grained bonds of length 2.39 Å. On this lattice, the angle between any two axes along the sides of the unit cell is 60°, and the lattice sites are identical to the hexagonal packing of hard spheres.

Energies. Both short-range intramolecular interactions and long-range intra- and intermolecular interactions are introduced into the current simulations. The short-range intramolecular interactions resulting from the local chain conformation are based on a RIS model for the unperturbed chain,[25] which incorporates the influence of partial charges. The RIS model for poly(A−A−B) chains, in which all bonds are subject to a symmetric 3-fold torsion potential with the nearest neighbor interdependence, is given by the following three statistical weight matrices for three successive bonds of type A−A, A−B, and B−A.

$$U_{AA} = \begin{bmatrix} 1 & \sigma_{BB} & \sigma_{BB} \\ 1 & \sigma_{BB} & \sigma_{BB}\omega_{AB} \\ 1 & \sigma_{BB}\omega_{AB} & \sigma_{BB} \end{bmatrix} \quad (1)$$

$$U_{AB} = \begin{bmatrix} 1 & \sigma_{AA} & \sigma_{AA} \\ 1 & \sigma_{AA} & \sigma_{AA}\omega_{AB} \\ 1 & \sigma_{AA}\omega_{AB} & \sigma_{AA} \end{bmatrix} \quad (2)$$

$$U_{BA} = \begin{bmatrix} 1 & \sigma_{AA} & \sigma_{AA} \\ 1 & \sigma_{AA} & \sigma_{AA}\omega_{AA} \\ 1 & \sigma_{AA}\omega_{AA} & \sigma_{AA} \end{bmatrix} \quad (3)$$

In the matrices, the rows and columns define the states of bonds $i-1$ and i, respectively. The three accessible rotational isomeric states for each bond are t, g^+, and g^-, used in this order in the matrices. The σ_{AA} and σ_{AB} are the statistical weights for the A−A and A−B type first-order interactions, and ω_{AA} and ω_{AB} represent the second-order interactions. They are calculated as Boltzmann factors using the energies listed in Table 1.[25] The short-range interactions determine the local chain conformation for an unperturbed chain. The detailed descriptions of the calculation of the conditional probability of bonds and the calculation of the short-range interactions were discussed in a previous publication,[26] in which a single PEO chain was studied by the same method.

The long-range interactions result from the bead−bead interactions, which are applied to all pairs of beads except for the nearest and second-nearest neighbors in the same molecule. The interactions of the directly bonded beads are a constant throughout the simulation and are ignored. The interactions of the second-nearest pairs are incorporated in the RIS model and are not counted again in the long-range interactions. The long-range interactions are obtained from a discretized form of the LJ potential, in which the second virial coefficient for polymers is evaluated similar to a nonideal gas using the Mayer f function.[27] The LJ parameters of many small molecules are tabulated in the literature.[28] However, the LJ parameters for two backbone atoms of PEO are not available since the pairs of two backbone atoms are not always the same. We use two different methods to estimate the σ and ϵ values.

The σ value is obtained by first noting that σ for propane is within 1% of $(3/2)^{1/3}\sigma_{ethane}$. Therefore, the required value of σ for a coarse-grained bead of PEO can be estimated from the data for methyl ether (CH_3-OCH_3, $\sigma = 4.307$ Å)[28] as

$$\sigma_{PEO} = (2/3)^{1/3}\sigma_{methyl\ ether} \quad (4)$$

from which $\sigma_{PEO} = 3.76$ Å.

The ϵ value is obtained by fitting the experimental bulk density of PEO at a suitable temperature from a series of simulations of free-standing PEO thin films that have different ϵ values. Since this work will study the threading of PEO in the melt, a temperature higher than the melting point of PEO (340 K)[29] should be chosen. Here, 373 K is selected to perform the simulations. The estimation of the ϵ value will be presented in the Results and Discussion section.

Moves. Single bead moves, which were used in our previous simulations for PE,[23] are supplemented by a set of multiple bead pivot moves[30] in order to improve the simulation efficiency. In a pivot move, bond vectors for a subchain of the original conformation are reversed to create a new configuration. A subchain with two to six beads is applied for pivot moves. A pivot move may permit crossing of chains, which greatly facilitates the rate at which the equilibrium of the degree of threading is achieved in the simulation. Since two to six bead pivot moves are incorporated into the simulation, the chain might cross through a cyclic molecule in some special cases, which restricts our simulation to the investigation of the properties in the equilibrium state instead of the dynamics of the threading process. For every Monte Carlo step (MCS), single bead moves and also multiple bead pivot moves are performed randomly. Every bead is tried once, on average, in both single bead moves and pivot moves. Therefore, a move of every bead is attempted twice, on average, within one MCS. Moves that cause double occupancy and collapses,[23] which are caused by the overlap of backbone atoms after the reverse-mapping of the coarse-grained chains to the fully atomistic description, have been prohibited. The Metropolis criteria[31] are applied to determine whether the move is made or not.

Film Formation. The film used in the prediction of the LJ parameters is initially constructed using an adaptation of the method of Misra et al.[32] to the lattice simulation, which has been demonstrated in our previous work on the high coordination lattice.[33−36] First, bulk NVT simulations are performed in a periodic box $L_x = L_y = 16$ and $L_z = 32$, which imposes the experimental density of a PEO melt on the system. After the equilibration of the melt, the periodic length of the box in one direction, which will be denoted by z, is increased by a factor of 3. This procedure eliminates the interaction of the parent chains with their images in the z direction. Therefore, the periodic boundary conditions are effective only in the remaining two directions. In

these simulations, the resulting lattice size of the periodic box is $L_x = L_y = 16$ and $L_z = 96$. The system includes 32 linear chains that are each 50 beads in length. After generating the new periodic boundary conditions, the system is equilibrated. The density of the model for the melt was imposed by the initial set of periodic boundary conditions, but the free-standing thin film selects its own bulk density at the simulated temperature. The experimental density at 373 K (1.06 g/cm^3)[37] is fit by changing the ϵ value. After obtaining the LJ parameters, all the simulations are performed in an *NVT* system.

System Description. The simulations for the determination of threading are performed in a periodic box with 20 unit lengths on each side of the lattice; i.e., $L_x = L_y = L_z = 20$. For all systems, a total of 1680 beads are put into this box to achieve the experimental density for PEO at 373 K.[37] Two series of systems are studied in the simulation. Series I studies the dependence of threading on the mass fraction of the cyclic molecules, X_c. In this series, the size of the linear and cyclic molecules are the same, $N = N_l = N_c = 21$; i.e., all the molecules have 21 beads on the lattice. These beads can be reverse-mapped into 42 backbone atoms, $CH_3(OCH_2$-$CH_2)_{13}OCH_3$ and 42-crown-14 for the linear and cyclic molecules, respectively. The mass fraction of the cyclic molecules, X_c, varies from 0.1, 0.175, 0.25, 0.50, 0.625, to 0.75. The number of the linear and cyclic molecules changes with the X_c, but the total number of molecules in the system remains the same at 80. Series II investigates the dependence of threading on the size of the cyclics, N_c. The mass fraction of cyclics, X_c, remains at 0.25 for different N_c. The size of the cyclic molecules changes from 12 beads (24-crown-8), 15 beads (30-crown-10), 21 beads (42-crown-14), to 30 beads (60-crown-20), but the 60 linear molecules each contain 21 beads.

For every system, the initial configuration contains cyclic molecules with the shape of a deformed rectangle, which are placed at different positions, and the linear chains are randomly distributed in the periodic box. Since unphysical collapses[23] can exist in the initial cyclic molecules, a short MC simulation is performed to remove this possible conformation. Next, a sufficiently long simulation is run until the system achieves equilibrium. After equilibration, an additional 8 million MCS are performed to evaluate the threading of the cyclic molecules by the linear chains. The configurations are recorded every 10 000 MCS.

Determination of Threading. Three kinds of cyclic molecules exist in general: (A) small cyclic molecules with very simple conformations in two dimensions, such as a circle or an ellipse; (B) intermediate cyclic molecules in which the structure changes from two to three dimensions, but still can be represented by a series of local planes in two dimensions; (C) very large cyclic molecules with very complicated shapes in three dimensions. In our simulations, the size of the cyclic molecules falls into group B, in which the three-dimensional shape of molecules can be divided into a series of two-dimensional planar structures. This assumption will be verified in the section of Chain Dimensions in the Results and Discussion, in which the conformations of the cyclic molecules are evaluated by the principal moments of the radius of gyration tensor. Here, we describe the procedure to determine the threading of such a cyclic molecule by a linear chain. On the high

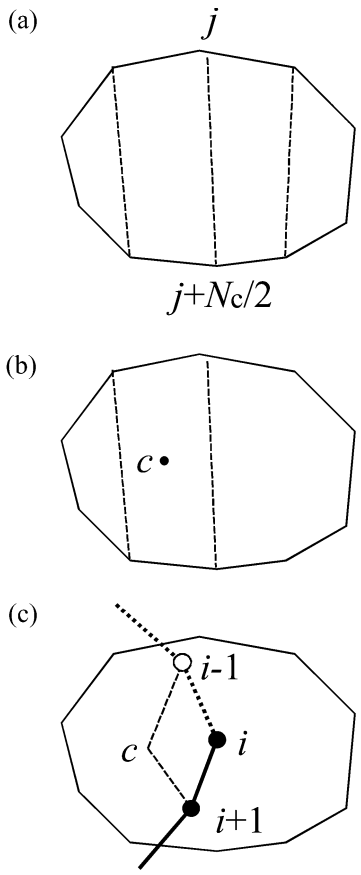

Figure 1. Schematic representation of the determination of threading: (a) define local planes, (b) find the center of a local plane, and (c) determine the threading.

coordination lattice, the cyclic has an even number of beads, N_c. (1) Find the $N_c/2$ distances between beads i and $i + N_c/2$, for i ranging from 1 to $N_c/2 - 1$. Sort the distances to find the shortest. Denote the beads that define this distance as beads j and $j + N_c/2$. Find all the lines between beads $j + k$ and $j + N_c/2 - k$ and between $j - k$ and $j + N_c/2 + k$, where $k = 1, 2, 3, ...$, until the number of beads between $j + k$ ($j - k$) and $j + N_c/2 - k$ ($j + N_c/2 + k$) is no more than 2. The schematic representation is depicted in Figure 1a. In this case, $k = 1$ and three lines are drawn. (2) Define a local plane between the pairs of the nearest dashed lines in Figure 1a, and find the center of the local plane, *c*, as shown in Figure 1b. (3) Find the nearest bead i from the center of the local plane. If bead i comes from a linear chain, determine the position of the $i - 1$ and $i + 1$ beads relative to the local plane. If the two beads are located at different sides of the local plane, the cyclic molecule is threaded (Figure 1c). This process is repeated for beads at successively greater distances from *c* until a bead is found from the same cyclic molecule. Then every local plane is checked to look for threading of other chains. Double counting of threading of a linear chain to the same cyclic molecule is excluded in this step. (4) Repeat steps 1−3 to check every cyclic molecule in the melt. The use of multiple bead pivot moves in the simulations allows the intercrossing of cyclics to occur. However, only the threading of a cyclic molecule by a linear chain is counted as a threading event. All the results are averaged for the configurations in 8×10^6 MCS.

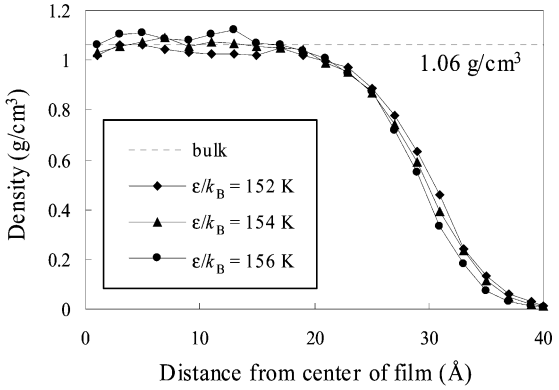

Figure 2. Density profile of a free-standing thin film of PEO at 373 K with $\sigma = 3.76$ Å and $\epsilon/k_B = 152$ (diamond), 154 (triangle), or 156 K (circle). The horizontal dashed line is the experimental bulk density.

Table 2. Shell Energies (kJ/mol) for $\sigma = 3.76$ Å and the Listed ϵ/k_B Values at 373 K

	$\epsilon/k_B = 152$ K	$\epsilon/k_B = 154$ K	$\epsilon/k_B = 156$ K
1st shell	8.108	8.113	8.117
2nd shell	−0.203	−0.213	−0.223
3rd shell	−0.334	−0.339	−0.343
4th shell	−0.066	−0.067	−0.068
5th shell	−0.017	−0.017	−0.018

Results and Discussion

Determination of LJ Parameters for the Model of PEO. As mentioned above, the value of σ was estimated as 3.76 Å. Free-standing PEO thin films are simulated to determine the value of ϵ to be used for the long-range interactions in the coarse-grained model. The simulations are a total of 2×10^6 MCS, with the first 1×10^6 MCS discarded as the equilibration of the system. The justification for using this number will be discussed in the next section. In Table 2, the discretized LJ interactions at 373 K for the first five shells are given for ϵ/k_B (k_B is the Boltzmann constant) of 152, 154, and 156 K when σ is 3.76 Å. The first shell is strongly repulsive since the distance between two beads, 2.39 Å, is smaller than the value of σ in the LJ potential. Both the second and third shells have attractive interaction, which leads to the cohesive nature of the polymer and the corresponding thin film. The fourth and higher shells are attractive, but less so than the third shell. The use of three shells improves the simulation efficiency with little sacrifice in accuracy. The density profiles for PEO thin films calculated for σ of 3.76 Å and ϵ/k_B of 152, 154, or 156 K are given in Figure 2. From this method, it is determined that the ϵ/k_B value of 154 K yields a cohesive film with a bulk density that most closely matches the experimental density of 1.06 g/cm^3.[37]

Equilibration of the System. Equilibration of the systems can be determined by evaluating the orientation autocorrelation functions (OACFS) defined using the end-to-end vector of the linear chain. The OACF is shown in Figure 3 for the system with a mass fraction of cyclics, X_c, of 0.5. The time constant for equilibration is the time required for the OACF to fall to $1/e$, and complete deconvolution of the end-to-end vectors from their initial orientations is obtained when the OACF reaches 0. For the system with $X_c = 0.5$, equilibrium conditions are satisfied in about 100 000 MCS. The OACFs for the other systems in the study, which are not shown here, show similar behavior.

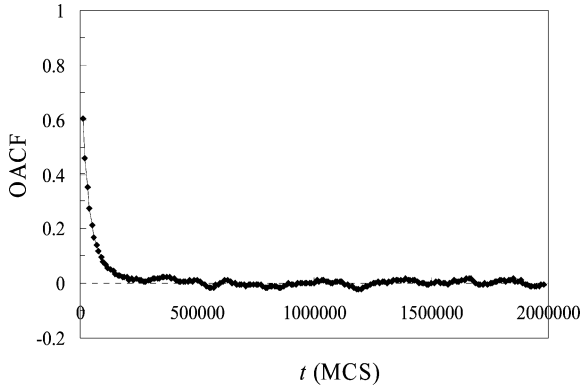

Figure 3. Orientation autocorrelation function (OACF) of the end-to-end vectors of the linear chain for the system with $X_c = 0.5$ and $N_c = N_l = 21$.

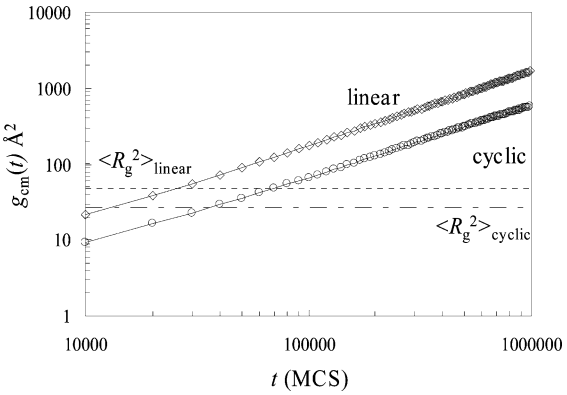

Figure 4. Mean-square displacement of the center-of-mass ($g_{cm}(t)$) of the linear chains (diamond) and cyclic molecules (circle) as a function of Monte Carlo step (MCS) for the system with $X_c = 0.5$ and $N_c = N_l = 21$. The horizontal dashed lines are the mean-square radius of gyration ($\langle R_g^2 \rangle$) of the linear chain and the cyclic molecule.

Table 3. Mean-Square Radius of Gyration ($\langle R_g^2 \rangle$) of the Linear Chains and the Cyclic Molecules with $N_c = N_l = 21$

X_c	$\langle R_g^2 \rangle_{linear}$, Å^2	$\langle R_g^2 \rangle_{cyclics}$, Å^2
0.100	47 ± 2	28 ± 2
0.175	47 ± 2	28 ± 1
0.250	48 ± 2	28 ± 1
0.500	47 ± 3	28 ± 2
0.625	47 ± 3	28 ± 1
0.750	47 ± 4	28 ± 2

In addition, the mean-square displacement of the center-of-mass ($g_{cm}(t)$) shown in Figure 4 for the system with $X_c = 0.5$ is evaluated to establish equilibrium conditions. This parameter is evaluated separately for the linear and cyclic molecules. When $g_{cm}(t)$ reaches the mean-square radius of gyration ($\langle R_g^2 \rangle$), the molecules have translated away from their initial positions. From Figure 4, it can be seen that equilibration of the system by 100 000 MCS is confirmed. Again, the other systems in the study show similar results for $g_{cm}(t)$ as the system in Figure 4. The OACF and $g_{cm}(t)$ indicate that the movement of the chains equilibrates rapidly so 1×10^6 MCS are used for equilibration and the chain dimensions are analyzed with only an additional 1×10^6 MCS. The average number of threading events, however, took longer to equilibrate, so an additional 8×10^6 MCS is necessary.

Chain Dimensions. The mean-square radius of gyration ($\langle R_g^2 \rangle$) of the linear chains and the cyclic molecules for the various X_c are given in Table 3. For

Table 4. Mean-Square Radius of Gyration, $\langle R_g^2 \rangle$ (Å^2), Principal Moments of the Radius of Gyration Tensor, $\langle L_1^2 \rangle$, $\langle L_2^2 \rangle$, $\langle L_3^2 \rangle$ (Å^2), and the Ratios $\langle L_2^2 \rangle / \langle L_1^2 \rangle$ and $\langle L_3^2 \rangle / \langle L_1^2 \rangle$ of the Cyclics with $N_l = 21$ and $X_c = 0.25$

N_c	$\langle R_g^2 \rangle_{cyclics}$	$\langle L_1^2 \rangle$	$\langle L_2^2 \rangle$	$\langle L_3^2 \rangle$	$\langle L_2^2 \rangle / \langle L_1^2 \rangle$	$\langle L_3^2 \rangle / \langle L_1^2 \rangle$
12 beads	13.5 ± 0.3	8.0	4.4	1.0	0.5	0.1
15 beads	18.5 ± 0.5	12.2	5.1	1.3	0.4	0.1
21 beads	28 ± 1	18.3	7.1	2.3	0.4	0.1
30 beads	41 ± 3	27.0	10.4	3.7	0.4	0.1

the different sizes of the cyclic molecules (N_c) that are evaluated, $\langle R_g^2 \rangle$ of the cyclic molecules are given in Table 4. Table 4 also contains the averaged principal moments of the radius of gyration tensor (for each conformation, $L_1^2 > L_2^2 > L_3^2$) and the ratios $\langle L_2^2 \rangle / \langle L_1^2 \rangle$ and $\langle L_3^2 \rangle / \langle L_1^2 \rangle$. The principal moments of the radius of gyration tensor provide a sense of whether the cyclic molecules are circular or oblong in nature and the degree of planarity. $\langle L_3^2 \rangle / \langle L_1^2 \rangle$ near zero would indicate a planar structure, and if this condition is met, $\langle L_2^2 \rangle / \langle L_1^2 \rangle$ approximately equal to one would indicate a circle. As expected, $\langle R_g^2 \rangle$ for the linear chains and the cyclic molecules are independent of X_c (Table 3). The values of $\langle L_2^2 \rangle / \langle L_1^2 \rangle$ and $\langle L_3^2 \rangle / \langle L_1^2 \rangle$ for the largest macrocycle compare well with published limiting values for macrocyclic molecules studied on a cubic lattice of 0.37 and 0.15, respectively.[38] The cyclics deviate slightly from planarity ($\langle L_3^2 \rangle / \langle L_1^2 \rangle$ values are slightly larger than 0) and are better described as ellipses than circles ($\langle L_2^2 \rangle / \langle L_1^2 \rangle$ values are about 0.4−0.5 and not as large as 1). This result confirms that the cyclic molecules fall into group B, which contains the intermediate cyclic molecules that can still be represented by a series of local planes in two dimensions.

Mixing Behavior of Cyclic Molecules and Linear Chains. The cyclic molecules and the linear chains are the same chemical species −(CH_2−CH_2−O)−. However, the cyclic molecules have the constraint that the head and tail beads are connected. This constraint may possibly influence the interactions of the system and cause some segregation to occur between the cyclic molecules and the linear chains. To verify that the system has not segregated, the intermolecular pair correlation function (PCF) is evaluated for the various systems included in the study. The function gives the probability of finding a particle A at a specified distance from another particle A defined by eq 5 on the high coordination lattice.[39]

$$g_{AA}(i) = \frac{\langle n_{AA}(i) \rangle}{(10i^2 + 2)V_A} \tag{5}$$

In eq 5, $n_{AA}(i)$ is the number occupancy of A in the ith shell from another A particle and V_A is the volume fraction of A in the entire system. Beads on the same chain are ignored in the evaluation of the intermolecular PCF.

For the system with $X_c = 0.5$, the intermolecular PCF as a function of shell number, which indicates the distance away from a given bead, is shown in Figure 5. Four PCFs are calculated. Two PCFs analyze similar pairs of molecules, such as linear−linear and cyclic−cyclic. The third one is for dissimilar pairs, linear−cyclic. Finally, the fourth, which is the total PCF, is for all pairs in the system. Although the values of the four PCFs in the second shell in Figure 5 are not the same, their differences do not exceed the sums of the standard deviations. We conclude the simulation provides little evidence for segregation of the cyclic and linear components of the system. This result indicates that a linear chain (cyclic molecule) is equally likely to find a cyclic molecule (linear chain) nearby as opposed to a linear chain (cyclic molecule). Although not shown here, the other systems show no differences in the intermolecular PCF.

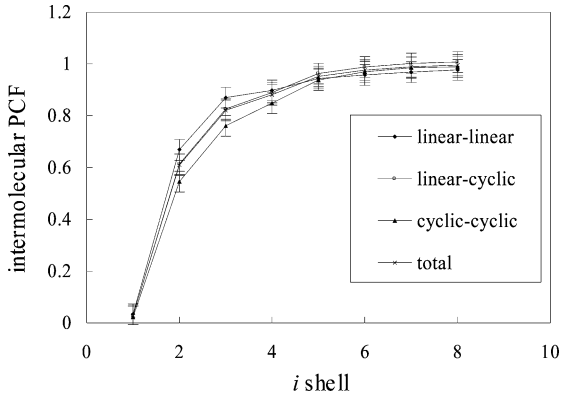

Figure 5. Four types of intermolecular pair correlation functions (PCFs) as a function of shell number for the system with $X_c = 0.5$ and $N_c = N_l = 21$.

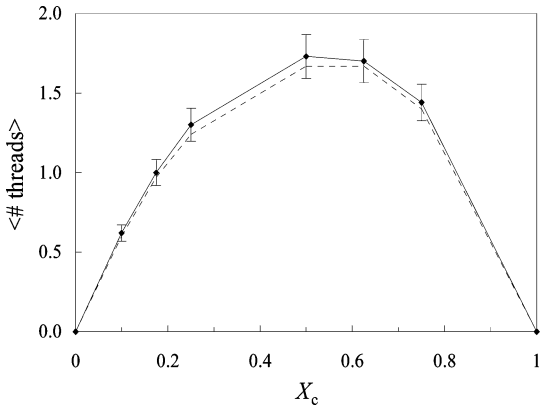

Figure 6. Average number of threading events in the data sets recorded (⟨no. of threads⟩) as a function of X_c with $N_c = N_l = 21$. The dashed line is the ⟨no. of threads⟩ with the multiple threading events subtracted from the total number of threading events.

Threading Events. In Figure 6, the relationship of the average number of threads in the data sets recorded (⟨no. of threads⟩) as a function of X_c is nearly symmetric about 0.5. This is the intuitive result that is expected and agrees qualitatively with experimental results on a series of "crown polyether" type cyclic molecules that were threaded with poly(ethylene glycol) chains.[40] As mentioned in the Simulation Method and Details section, intercrossing of cyclics can occur in the simulations. To verify that ⟨no. of threads⟩ has not been influenced by the incorporation of multiple bead pivot moves, a simulation for the system with $X_c = 0.5$ that contained only single bead moves for the cyclic molecules was performed. To quickly achieve equilibrium, the linear chains were allowed both single and multiple bead pivot moves. The final average number of threading events

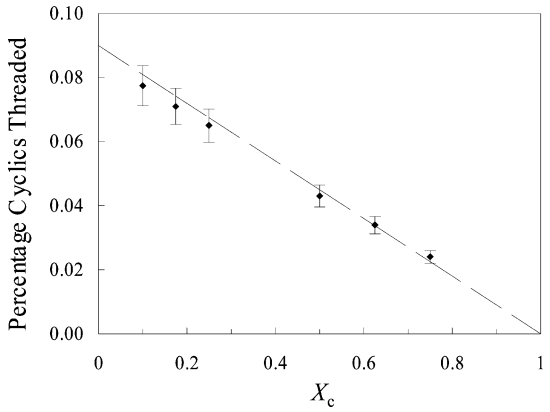

Figure 7. Percentage of cyclic molecules threaded as a function of X_c with $N_c = N_l = 21$. The dashed line is a straight line fit to the data.

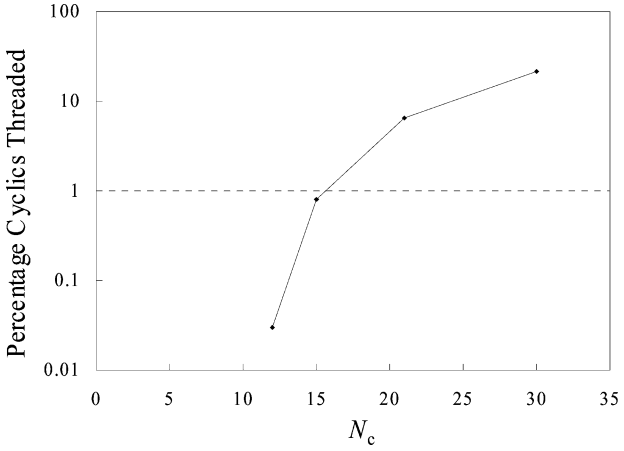

Figure 8. Percentage of cyclic molecules threaded as a function of N_c with $X_c = 0.25$ and $N_l = 21$. The dashed horizontal line indicates a percentage of 1%.

was 1.73 ± 0.07 for the system allowing both types of moves for the cyclics and 1.78 ± 0.09 for the system with single bead moves for the cyclics.

Replotting the results of Figure 6 as a percentage of cyclic molecules threaded yields a decreasing linear dependence on X_c, as shown in Figure 7. A straight line can be fit to the data. The extrapolation to $X_c = 0$ implies that about 9% of the cyclics with $N_c = 21$ would be threaded in a cyclic:linear mixture that is very dilute in the cyclic component.

Figure 8 shows the percentage of cyclic molecules threaded as a function of N_c, the size of the cyclic molecules, when X_c is held constant at 0.25. The percentage of cyclic molecules threaded increases with an increase in the number of atoms in the cyclic but falls to less than 1% when N_c is less than 16. Above 21 beads, the increase in the percentage of cyclic molecules threaded with the size of the cyclic molecules is much slower than the increase observed between 15 and 21 beads.

In Figure 9, the percentage of cyclic molecules threaded for PEO in the current study is compared to the results reported in the literature for PDMS.[13,14,41] The results from the study by DeBolt and Mark are using model II with a torus radii of 0.35 nm.[13] The results of Joyce, Hubbard, and Semlyen are obtained with the 0.74 nm threading chain.[14] For the smaller cyclics containing 24, 30, and 42 backbone atoms, the results for PEO are similar to those reported for PDMS. The percentage of

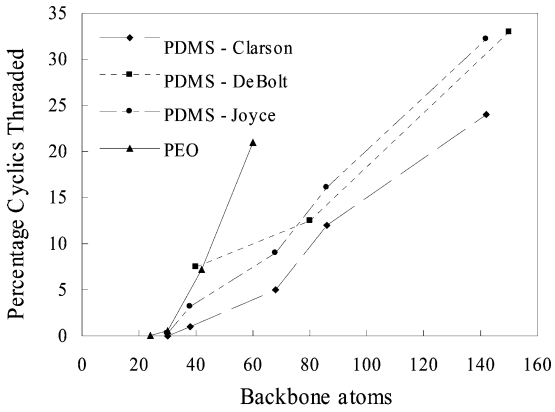

Figure 9. Percentage of cyclic molecules threaded for PEO from the current study and reported values for PDMS from RIS theory[13,14] and from experimental results[41] as a function of the number of backbone atoms.

cyclic molecules threaded for the largest cyclic PEO molecules with 60 backbone atoms was much larger than the percentage reported for PDMS.

Our simulations and the experimental results differ in the definition of threading. In our simulations, a threading event is counted whenever beads i and $i + 1$ of a linear chain are on opposite sides of the mean plane defined for a ring. Penetration of the mean plane of the ring by a single bead is sufficient to produce a threading event. In the experiments of Clarson et al.,[41] a mixture of 15% cyclic PDMS and 85% linear hydroxy-terminated PDMS was subjected to end-linking of the linear species by reaction with tetraethyl orthosilicate, thereby producing a network from the reaction of the hydroxyl groups at the ends of the linear component. After completion of the reaction, the cyclics that could not be extracted from the cross-linked sample were counted as threaded.

There are two reasons to expect that our definition of threading should produce the larger population of threaded cyclics. First, the extent of the penetration of the linear species through a ring may affect the probability that its hydroxyl terminus can react with a bulky group such as tetraethyl orthosilicate or a partially reacted tetraethyl orthosilicate. If the probability of this reaction is suppressed when a linear chain barely penetrates the mean plane of the ring, the experiment will count fewer successful threading events than our simulation. Second, although Clarson et al.[41] endeavored to minimize the number of dangling ends in their cross-linked sample, any rings threaded by dangling ends would be extractable and therefore would not be counted as threading events by their method. Such rings would, however, be counted as threading events in our simulations.

Finally, the hydroxyl terminus of the linear PDMS species in the experiments of Clarson et al.[41] implies that the end groups of their linear chains interact differently with the surroundings than do the repeat units in the interior of the PDMS chain. If treated as a chain of beads with one bead per monomer unit, their system would require different values of the LJ σ and ϵ for interior beads and for hydroxyl-terminated end beads. In contrast, our simulation is performed with linear chains that reverse map to methyl-terminated linear chains. Our end beads are treated with the same σ and ϵ as the internal beads.

When they performed their simulations, it was not feasible for DeBolt and Mark[13] to look directly at

Table 5. Occurrence of Multiple Threading

X_c or N_c	type 1: 1 L & 2 C[a]	type 2: 1 C & 2 L[b]	type 2: 1 C & 3 L[c]	total of type 1 and type 2
$N_c = 21$				
0.10	0	13	0	13
0.175	6	19	0	25
0.25	12	35	0	47
0.50	27	21	0	48
0.625	21	11	0	32
0.75	28	2	0	30
$X_c = 0.25$				
12 beads	0	0	0	0
15 beads	0	0	0	0
21 beads	12	35	0	47
30 beads	36	191	5	232

[a] One linear chain threading two cyclic molecules. [b] One cyclic molecule threaded by two linear chains. [c] One cyclic molecule threaded by three linear chains.

equilibrated bulk PDMS systems, as we have done with coarse-grained PEO. Therefore, they inferred the likely amount of threading in PDMS from the study of a representative sample of isolated rings. Their preferred method, and the one for which results are depicted in Figure 9, centered a torus on each monomer unit in turn in the ring. The torus was assigned a radius appropriate for the cross section of a linear PDMS chain. If the torus was completely unoccupied by other atoms from the ring, there was an open path through the ring of sufficient size to accommodate a linear chain, and the ring was counted as being threaded. However, the threading event in reality would not require that the entire torus be vacant; it would suffice that merely the appropriate segment of the torus be vacant, as was recognized by DeBolt and Mark. However, since the "appropriate segment" of the torus was not easily defined in their work, they instead employed the more severe requirement that the entire torus be vacant. They will tend to undercount the number of successful threading events for this reason. The undercounting will be minimal for very small cyclics, with conformations accurately described by a circle, but will become a more serious problem for larger rings with more convoluted conformations. Our simulation corresponds to the more accurate requirement that only the "appropriate segment" of the torus need be vacant, and therefore our method will count more successful threading events than the method of DeBolt and Mark, with the difference in the two methods increasing as the degree of polymerization of the ring increases.

Multiple Threading. Table 5 lists the occurrence of multiple threading, which can be defined as the following two types: (1) a linear chain that threads more than one cyclic molecule or (2) a cyclic that is threaded by more than one linear chain. As expected, as the size of the cyclic increases, the number of multiple threading events increases. The highest number of linear chains that threaded a single cyclic molecule is three. This event is observed only in the largest cyclic molecule that was evaluated, N_c of 30 beads. In addition, the type of threading, type 1 or type 2, is dependent on the mass fraction of cyclics, X_c. The first six lines of Table 5 confirm the expectation that type 1 multiple threading goes to zero as $X_c \rightarrow 0$ and type 2 multiple threading goes to zero as $X_c \rightarrow 1$. The last four lines present information that is not so apparent from intuition alone. Multiple threading is first observed in the cyclic with 21 beads (42-crown-14), and the first detection of threading of a cyclic by three linear chains is made when the cyclic has 30 beads (60-crown-20). In Figure 6, the dashed line indicates the average threading as a function of X_c after subtracting out the number of multiple threading events from the total number of threading events. Within simulation error, the average number of threading events does not change.

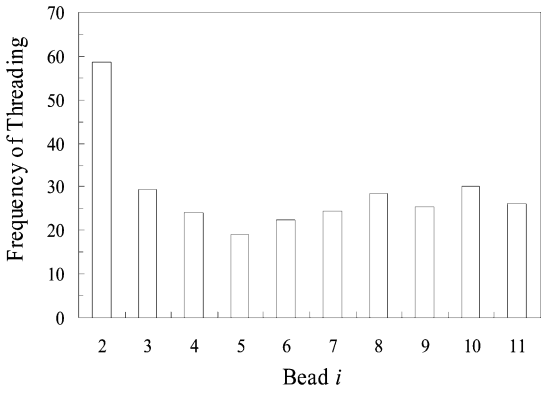

Figure 10. Frequency of threading for a given bead *i* as defined in the text.

Distribution of Threading Sites along the Linear Chain. In Figure 10, the number of times that a given bead *i* in the linear chain was the bead closest to the center of the local plane (see Determination of Threading described above) is shown for the system with $X_c = 0.5$ and $N_c = N_l = 21$ beads. Similar results are obtained for the other systems in the study. In the figure, bead $i = 2$ includes bead 2 and bead 20, bead $i = 3$ includes bead 3 and bead 19, and so on, with bead 11 being the center of the linear chain. Beads 1 and 21 are ignored since our definition of threading at bead *i* requires the existence of bead $i \pm 1$. A preference, approximately 2 to 1, for the second bead from the end of the chain (either bead 2 or 20) as bead *i* is observed. This result shows that there is a slight end effect that forms threading near a chain end. In addition, Figure 10 shows that the cyclic molecules are not located only at the ends of the linear chain, but the cyclic molecules are equally likely to be found at the center of the linear chain or anywhere along the chain, except as noted above for the second bead from the end.

Conclusions

The dependence of threading on the mass fraction, X_c, and the size, N_c, of the cyclics is determined. A coarse-grained model for PEO is constructed and validated for this specific system. For the model on the high coordination lattice, the LJ parameters σ and ϵ/k_B are estimated at 3.76 Å and 154 K, respectively. This model allows for rapid equilibration of the system.

A method to detect threading in cyclics that have instantaneous conformations differing from a circle is described. The percentage of cyclic molecules threaded is described as a linear function of X_c and falls to less than 1% when the cyclic decreases in size to 30-crown-10. A nearly order of magnitude increase in the percentage of cyclics threaded is observed between 30-crown-10 and 42-crown-14. However, the rate of increase of the percentage of cyclics threaded is much slower for cyclics larger than 42-crown-14. The simulations suggest that it is impractical to seek spontaneous threading of cyclics much smaller than 30-crown-10. Multiple threading has its onset at 42-crown-14. Finally, a weak end effect occurs that forms slightly higher threading near a chain end.

Acknowledgment. This work was supported by NASA John H. Glenn research center.

References and Notes

(1) Schill, G. *Catenanes, Rotaxanes and Knots*; Academic Press: New York, 1971.
(2) Dietrich-Buchecker, C. O.; Sauvage, J.-P. *Chem. Rev.* **1987**, *87*, 795.
(3) Preece, J. A.; Stoddart, J. F. *Nanobiology* **1994**, *3*, 149.
(4) Gibson, H. W.; Bheda, M. C.; Engen, P. T. *Prog. Polym. Sci.* **1994**, *19*, 843.
(5) Amabilino, D. B.; Stoddart, J. F. *Chem. Rev.* **1995**, *95*, 2725.
(6) Raymo, F. M.; Stoddart, J. F. *Trends Polym. Sci.* **1996**, *4*, 208.
(7) Amabilino, D. B.; Raymo, F. M.; Stoddart, J. F. In *Comprehensive Supramolecular Chemistry*; Lehn, J.-M., Ed.; Pergamon Press: Oxford, England, 1996; Chapter 3.
(8) Vögtle, F.; Dünnwald, T.; Schmidt, T. *Acc. Chem. Res.* **1996**, *29*, 451.
(9) Chambron, J. C. *Perspect. Supramol. Chem.* **1999**, *5*, 225.
(10) Breault, G. A.; Hunter, C. A.; Mayers, P. C. *Tetrahedron* **1999**, *55*, 5265.
(11) *Molecular Catenanes, Rotaxanes and Knots*; Sauvage, J. P.; Dietrich-Buchecker, C., Eds.; Wiley-VCH Verlag GmbH: Weinheim, 1999.
(12) Frisch, H. L.; Wasserman, E. *J. Am. Chem. Soc.* **1961**, *83*, 3789.
(13) DeBolt, L. C.; Mark, J. E. *Macromolecules* **1987**, *20*, 2369.
(14) Joyce, S. J.; Hubbard, R. E.; Semlyen, J. A. *Eur. Polym. J.* **1993**, *29*, 305.
(15) Ha, Y. L.; Chakraborty, A. K. *Chem. Eng. Sci.* ***1994***, *49*, 2859.
(16) Amabilino, D. B.; Ashton, P. R.; Balzani, V.; Brown, C. L.; Credi, A.; Fréchet, J. M. J.; Leon, J. W.; Raymo, F. M.; Spencer, N.; Stoddart, J. F.; Venturi, M. *J. Am. Chem. Soc.* **1996**, *118*, 12012.
(17) Grabuleda, X.; Jaime, C. *J. Org. Chem.* **1998**, *63*, 9635.
(18) Leigh, D. A.; Troisi, A.; Zerbetto, F. *Angew. Chem., Int. Ed.* **2000**, *39*, 350.
(19) Herrmann, W.; Keller, B.; Wenz, G. *Macromolecules* **1997**, *30*, 4966.
(20) Schalley, C. A.; Silva, G.; Nising, C. F.; Linnartz, P. *Helv. Chim. Acta* **2002**, *85*, 1578.
(21) Pugh, C.; Bae, J.-Y.; Scott, J. R.; Wilkins, C. L. *Macromolecules* **1997**, *30*, 8139.
(22) Rapold, R. F.; Mattice, W. L. *J. Chem. Soc., Faraday Trans.* **1995**, *91*, 2435.
(23) Doruker, P.; Mattice, W. L. *Macromolecules* **1997**, *30*, 5520.
(24) Doruker, P.; Mattice, W. L. *Macromol. Theory Simul.* **1999**, *8*, 463.
(25) Abe, A.; Tasaki, K.; Mark, J. E. *Polym. J.* **1985**, *17*, 883.
(26) Doruker, P.; Rapold, R. F.; Mattice, W. L. *J. Chem. Phys.* **1996**, *104*, 8742.
(27) Cho, J.; Mattice, W. L. *Macromolecules* **1997**, *30*, 637.
(28) *The Properties of Gases and Liquids*, 4th ed.; Reid, R. C., Prausnitz, J. M., Poling, B. E., Eds.; McGraw-Hill: New York, 1987; p 733.
(29) Yuan, Q. W. In *Polymer Data Handbook*; Mark, J. E., Ed.; Oxford University Press: Oxford, 1999; p 546.
(30) Clancy, T. C.; Mattice, W. L. *J. Chem. Phys.* **2000**, *112*, 10049.
(31) Metropolis, N.; Rosenbluth, A. W.; Rosenbluth, M. N.; Teller, A. H.; Teller, E. *J. Chem. Phys.* **1953**, *21*, 1087.
(32) Misra, S.; Fleming, P. D., III; Mattice, W. L. *J. Comput.-Aided Mater. Des.* **1995**, *2*, 101.
(33) Doruker, P.; Mattice, W. L. *Macromolecules* **1998**, *31*, 1418.
(34) Doruker, P.; Mattice, W. L. *Macromolecules* **1999**, *32*, 194.
(35) Xu, G.; Mattice, W. L. *J. Chem. Phys.* **2002**, *116*, 2277.
(36) Xu, G.; Mattice, W. L. *J. Chem. Phys.* **2002**, *117*, 3440.
(37) Orwoll, R. A. In *Physical Properties of Polymers Handbook*; Mark, J. E., Ed.; American Institute of Physics: Woodbury, 1996; p 82.
(38) Solc, K. *Macromolecules* **1973**, *6*, 378.
(39) Xu, G.; Mattice, W. L. *Polymer* **2002**, *43*, 7007.
(40) Agam, G.; Graiver, D.; Zilkha, A. *J. Am. Chem. Soc.* **1976**, *98*, 5206.
(41) Clarson, S. J.; Mark, J. E.; Semlyen, J. A. *Polym. Commun.* **1986**, *27*, 244.

MA0301855